


Article

Copula-Based Abrupt Variations Detection in the Relationship of Seasonal Vegetation-Climature in the Jing River Basin, China

Jing Zhao ¹, Shengzhi Huang ^{1,*}, Qiang Huang ¹, Hao Wang ², Guoyong Leng ^{3,4}, Jian Peng ^{5,6,7}  and Haixia Dong ¹

¹ State Key Laboratory of Eco-hydraulics in Northwest Arid Region of China, Xi'an University of Technology, Xi'an 710048, China

² State Key Laboratory of Simulation and Regulation of Water Cycle in River Basin, China Institute of Water Resources and Hydropower Research, Beijing 100038, China

³ Key Laboratory of Water Cycle and Related Land Surface Processes, Institute of Geographic Sciences and Natural Resources Research, Chinese Academy of Sciences, Beijing 100101, China

⁴ Environmental Change Institute, University of Oxford, Oxford OX1 3QY, UK

⁵ School of Geography and the Environment, University of Oxford, Oxford OX1 3QY, UK

⁶ Department of Geography, University of Munich (LMU), 80333 Munich, Germany

⁷ Max Planck Institute for Meteorology, 20146 Hamburg, Germany

* Correspondence: huangshengzhi@xaut.edu.cn; Tel.: +86-156-8606-0577

Received: 22 May 2019; Accepted: 5 July 2019; Published: 9 July 2019



Abstract: Understanding the changing relationships between vegetation coverage and precipitation/temperature (P/T) and then exploring their potential drivers are highly necessary for ecosystem management under the backdrop of a changing environment. The Jing River Basin (JRB), a typical eco-environmentally vulnerable region of the Loess Plateau, was chosen to identify abrupt variations of the relationships between seasonal Normalized Difference Vegetation Index (NDVI) and P/T through a copula-based method. By considering the climatic/large-scale atmospheric circulation patterns and human activities, the potential causes of the non-stationarity of the relationship between NDVI and P/T were revealed. Results indicated that (1) the copula-based framework introduced in this study is more reasonable and reliable than the traditional double-mass curves method in detecting change points of vegetation and climate relationships; (2) generally, no significant change points were identified during 1982–2010 at the 95% confidence level, implying the overall stationary relationship still exists, while the relationships between spring NDVI and P/T, autumn NDVI and P have slightly changed; (3) teleconnection factors (including Arctic Oscillation (AO), Pacific Decadal Oscillation (PDO), Niño 3.4, and sunspots) have a more significant influence on the relationship between seasonal NDVI and P/T than local climatic factors (including potential evapotranspiration and soil moisture); (4) negative human activities (expansion of farmland and urban areas) and positive human activities (“Grain For Green” program) were also potential factors affecting the relationship between NDVI and P/T. This study provides a new and reliable insight into detecting the non-stationarity of the relationship between NDVI and P/T, which will be beneficial for further revealing the connection between the atmosphere and ecosystems.

Keywords: copula-based method; NDVI and precipitation/temperature; change points; teleconnection factors; double cumulative curve method

1. Introduction

Terrestrial vegetation is the most important component of an ecosystem due to its critical roles in energy budget, water, and biogeochemical cycle of the earth ecosystem through photosynthesis and

transpiration, and it can change the climate system and alter the land surface [1–4]. From another perspective, the variation of vegetation coverage is a reflection of corresponding climatic conditions such as precipitation and temperature [5,6]. It is well known that climate changes have been characterized by an increase of 0.85 °C global surface temperature during 1880–2010, which was documented by the Intergovernmental Panel on Climate Change (IPCC) Fifth Assessment Report [7]. Accordingly, this warming trend provides abundant thermal energy to regulate the inner biogeochemical processes of plants, thus affecting vegetation coverage, vegetation health, and vegetation productivity [8–11].

There is increasing evidence that vegetation growth has a relationship with many physiographic and climatic attributes such as soil moisture [12,13], leaf area index [14], and regional evapotranspiration [15,16]. Among the climatic factors, precipitation (P) and temperature (T) have been proven to be the main factors influencing the distribution and composition of vegetation. Several studies have investigated the relationship between the Normalized Difference Vegetation Index (NDVI) and P/T [17–19]. For instance, Wen et al. [20] reported that vegetation was closely related to asymmetric warming, and it responded to the asymmetric warming with nearly one year delays at a global scale. Ji and Peters [21] investigated the relationship between vegetation and rainfall in the northern and central Great Plains of the USA and found the time lag and accumulative effects of rainfall on vegetation. All the above-mentioned studies have revealed the relationships between NDVI and P/T, and have confirmed the time lag effects between NDVI and P/T. However, under the background of a changing environment, the stationarity of the relationship between NDVI and P/T might be altered, and this could strongly affect the accuracy of the prediction models for vegetation based on its correlation with climatic factors. Nonetheless, fewer comparative studies have identified the change points in the relationship between NDVI and P/T. Hence, exploring the non-stationarity of the relationship between NDVI and climatic factors is the main objective in the present study, which helps to further understand the mechanisms of vegetation dynamic.

Nevertheless, some statistical methods have been adopted to investigate the change points of the binary relationship. Among multiple statistical methods, the correlation coefficient method was commonly employed in previous studies [22–24]. However, the correlation coefficient method which directly reflects the general trend and the strength of the bivariate relationship assumes that the relationships of the two time series are monotonous and stationary [25]. Due to the complexity of ecosystems, the relationship between NDVI and climatic factors is affected by multiple factors and characterized by nonlinearity which will cause the correlation coefficient method to assume that stationarity is not applicable here, and fail to capture the change points in the relationship between variables. Besides, conceptual models were utilized in some previous studies to identify change points. Lee et al. [26] proposed 12 conceptual model structures for the regionalization of the precipitation-runoff relationship on 28 UK catchments. In the Birkinshaw and Bathurst [27] study, a spatially distributed model was used to investigate the variation of relationship between sediment yield and river basin area. However, those model-based methods require a large amount of input data, and it is difficult to determine their parameters. Copula functions, which can represent the dependency structure between variables by constructing the joint distributions of related variables and reflect the linear and nonlinear relationship between variables, overcome the shortcomings of previous methods. As copula functions can directly deal with non-stationarity, and are characterized by flexibility and less limitation on the types of marginal distributions to be connected, they have been widely used in the financial field and are now increasingly adopted in hydro-meteorology fields to detect the abrupt change of the relationships between two variables. Gu et al. [28] developed a new regional contagion detection method based on the vine copula to conduct a study on financial contagion. Huang et al. [29] detected the possibly changing relationship between precipitation and temperature in the Wei River Basin, China, by copula functions. However, the copula function has not been used to identify the change point of the relationship between vegetation and meteorological variables. Therefore, this study seeks to utilize copula functions to present the relationship between NDVI and P/T and simultaneously detect the change points of their relationships [30].

Furthermore, various studies have been conducted to investigate the possible connection between atmospheric teleconnection factors and vegetation growth and climatic factors [31–33]. For instance, Li et al. [34] documented that the spatial patterns of NDVI have closer connections to El Niño over Eurasia. Cavazos [35] presented that changes in the circulation related to Arctic Oscillation (AO) strongly controlled the winter extreme precipitation in Balkans. Additionally, Wu and Wang [36] evaluated the impact of AO and Siberian High on the East Asian winter monsoon, and they concluded that higher winter air temperature occurs over East Asia during the positive AO phase. Nevertheless, considerable studies previously have focused on exploring the impacts of climatic and teleconnection factors on the individual components such as NDVI, P, and T, but the underlying causes for the variations in the relationship between NDVI and P/T by the climatic and atmospheric teleconnection factors (e.g., soil moisture (SM), potential evapotranspiration (PET), AO, Pacific Decadal Oscillation (PDO), El Niño–Southern Oscillation (ENSO), and sunspots) across seasons still lacks detection. Moreover, the dominant drivers leading to variations in the relationship between vegetation and climatic factors have not been revealed. Thereby, a greater understanding of how each teleconnection factor influences the relationship between NDVI and P/T will be fully explored in this present study.

The Jing River Basin (JRB), which belongs to the Loess Plateau, China, is a typical eco-environmentally vulnerable region in the world. The Loess Plateau is characterized by a highly erosive loess layer, which leads to serious degradation of the ecological environment in the Loess Plateau after centuries of unsustainable agricultural production and population explosion. Therefore, the Chinese government has carried out a series of ecological restoration projects since the 1970s to solve the serious environmental and ecological problems. Among them, the “Grain for Green” project implemented since 1999 has received remarkable feedback. The vegetation condition has been greatly improved, which might influence the relationship between NDVI and P/T. Consequently, it is necessary to investigate the relationship between NDVI and P/T in the JRB. Based on the long-term NDVI data and hydrometeorological observations, we aim (1) to introduce a copula-based framework for the change points detection and verify the reliability and superiority of this method; (2) to identify the change points of the relationship between seasonal NDVI and P/T; (3) to examine the impact of climate change on the variations of the relationships between NDVI and P/T and to determine the dominant driver of the seasonal variations. Generally, this study provides a new and reliable insight into detecting the non-stationarity of the relationship between NDVI and P/T, which will be beneficial for further revealing the connection between the atmosphere and ecosystems.

2. Materials and Methods

2.1. Study Area

The JRB (106.2°E–109.1°E, 34.8°N–37.4°N) is a typical arid and semi-arid region which is located in the southwest of the Loess Plateau (Figure 1). As the second level tributary of the Yellow River Basin (YRB), the JRB covers a total area of approximately 4.54×10^4 km². Located in the transitional zone between the temperate semi-humid and temperate semi-arid regions, the JRB experiences a typical temperate continental monsoon climate and the mean annual precipitation is 545 mm. The mean temperature in the coldest month ranges from -3 to -1 °C, whilst that in the hottest month varies from 23 to 26 °C [37]. Overall, the JRB is characterized by abundant precipitation and high temperature in summer and by rare precipitation and low air temperature in winter. Loessial soil and dark loessial soil are two typical types of soil which are highly erodible and widely distributed in the study areas [38,39]. Nearly 60% of annual precipitation is concentrated in the flood season (from June to September), which makes water loss and soil erosion occur frequently in the JRB. Thus, the JRB is widely known as a sediment-laden basin with 2.6×10^8 t sediment transporting into the YRB on average [40]. Accordingly, the ecological environment is extremely fragile and the vegetation coverage is sparse in the JRB.

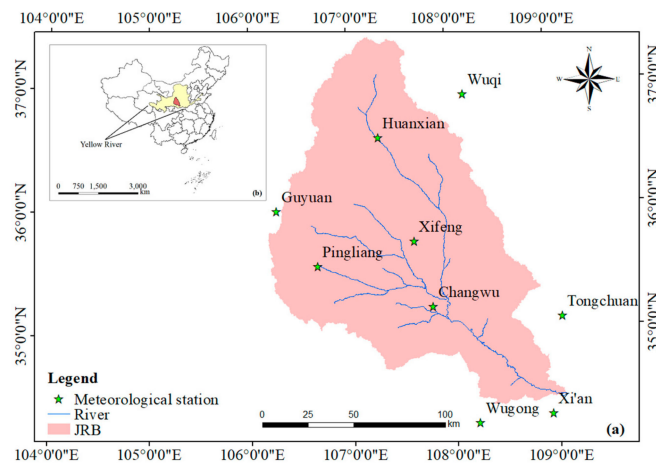


Figure 1. Location of the Jing River Basin. (a) The basin map of the Jing River Basin; (b) location of the Jing River Basin in the Yellow River Basin, China.

2.2. Datasets

The NDVI is a vegetation indicator which reflects the vegetation coverage by separating vegetation from water and soil. In this study, we focused on the vegetation dynamics during 1982–2010. The NDVI remote sensing data was obtained from the US National Oceanic and Atmospheric Administration’s (NOAA) Advanced Very High Resolution Radiometer (AVHRR) (<https://nex.nasa.gov/nex/projects/1349/>). Due to the poor vegetation coverage in winter on the Loess Plateau [41], we only focused on spring, summer, and autumn vegetation in the present study. Moreover, in order to avoid data changes caused by cloud cover and other uncertain factors, we used the maximum value of each season to represent the seasonal vegetation condition. In the current study, the gridded NDVI data within the JRB was averaged for use.

Additionally, the point daily meteorological data covering 1982–2010, including daily maximum and minimum temperature, wind speed, air pressure, sunshine duration, relative humidity, and daily mean precipitation, were recorded by nine meteorological stations and the dataset were obtained from the National Climate Center (NCC) of the China Meteorological Administration (CMA). Recommended by the World’s Food and Agriculture Organization (FAO) in 1998, the Penman–Menteith method was used to calculate the point PET. Based on the point meteorological data, the regional P and PET in the JRB were calculated by the Thiessen polygon method which is a widely used technique in deriving regional P and PET [42].

Besides, in order to examine the correlations between climatic/large-scale atmospheric circulations and relationships between seasonal NDVI and P/T, the PET, SM, AO, PDO, Niño 3.4, and sunspots were also employed in this study. The gridded monthly SM data was estimated by the Variable Infiltration Capacity (VIC) model. In the current study, the gridded SM data within the JRB area was averaged for use. AO data were collected from the NOAA National Climatic Data Center (http://www.cpc.ncep.noaa.gov/products/precip/CWlink/daily_ao_index/ao_index.html), and the monthly PDO index was downloaded from the Tokyo Climate Center (<http://ds.data.jma.go.jp/tcc/tcc/products/elnino/decadal/pdo.html>). The monthly Niño 3.4 index was used to represent ENSO activities which were acquired from the NOAA Earth System Research Laboratory (<http://www.esrl.noaa.gov/psd/data/correlation/nina34.data>). Monthly sunspot indexes were obtained from the National Geophysical Data Center (NGDC) of the NOAA (https://www.esrl.noaa.gov/psd/gcos_wgsp/Timeseries/SUNSPOT/).

Furthermore, in order to explore the correlations between human activities and the relationship between NDVI and P/T, the effective irrigated area data of the Shaanxi Province, Gansu Province, and Ningxia District were collected from the Ministry of Agriculture and Rural Affairs of the People’s Republic of China (<http://zzys.agri.gov.cn/nongqing.aspx>). Based on the province data and the area weight of the JRB in each province, the effective irrigated area data in the JRB was obtained. Moreover,

land use maps (1:100,000) for six periods (1980, 1990, 1995, 2000, 2005, and 2010) were used in the current study. They were generated from Landsat Thematic Mapper (TM) images using visual interpretation and obtained from the Resource and Environment Data Cloud Platform of Chinese academy of sciences (<http://www.resdc.cn/data.aspx?dataid=176>) which provides accurate, abundant, reliable, dynamic geographic information sources by collecting dynamic observations of the earth from the ‘Spot’ satellites. According to the national standard of classification of land use status (GB/t21010-2007), the land use types were classified into farmland, forestland, grassland, water bodies, construction land, and unused land.

2.3. Trend Analysis

The original Mann–Kendall (MK) test is a popular non-parametric method for accessing the trends of hydrometeorological variables [43]. However, the MK method is based on the uncorrelated data and the results are easy to be affected by the persistence of time series. Therefore, Hamed and Rao [44] proposed a modified Mann–Kendall (MMK) method by containing the lag- i autocorrelation to remove the persistence. In this study, we applied the MMK test to explore the variations trends of vegetation cover and precipitation/temperature, and the significance level was set at 0.05. The detailed computational processes can be referred to our previous research [45,46].

2.4. A Copula-Based Framework for Identifying the Change Points of the Relationship between NDVI and P/T

To identify the change points of the relationship between seasonal NDVI and P/T, a copula-based framework is implemented in the current study. This framework contains of such steps as fitting the most appropriate marginal distributions, selecting the joint distributions, and identifying the change points.

2.4.1. Marginal Distribution

A marginal distribution is the projection of the joint distribution of a set of random variables onto a subspace which is defined by a subset of components. Since the seasonal NDVI, P, and T series utilized in the current study are continuous, some parametric distributions (such as Gamma distribution, Generalized Extreme Value (GEV) distribution, and lognormal distribution), which are frequently applied to fit the distribution of hydrometeorological time series, were applicable in this study [47]. Besides, the parameters of these distributions were evaluated by the Maximum Likelihood Estimation (MLE) method [48]. Since the errors in marginal distributions can be amplified in the determination of joint distribution, efforts should be made to fit marginal distributions as accurately as possible. Based on the research of Wilks [49], the goodness-of-fit of each individual distribution was evaluated by the Kolmogorov–Smirnov (K-S) test, thus the most suitable distribution for each individual NDVI and P/T was obtained.

2.4.2. Joint Distribution

The copula function can construct the joint probability distribution of the multivariate hydrologic series through integrating their corresponding marginal distributions. The formula of the copula is expressed as follows:

$$C(u, v) = \varphi^{-1}(\varphi(u), \varphi(v)), \quad (1)$$

where φ denotes the convex function; and u and v represent the two variables.

Generally, the Archimedean copulas are widely used for the frequency analysis of multivariate hydrologic series due to their easily constructed characteristics and the numerous available copula families [50]. In order to avoid over-parameterization and easily estimate the parameter, Gumbel, Frank, and Clayton copulas which were widely known as three simple Archimedean copulas, were chosen to assess the joint probability distribution of the NDVI and climate factors in the JRB. Acquiring the generating function from multivariate observation data is the crucial step to determine a copula

which was shown in detail in the study of Genest and Rivest [51]. In the present study, the minimum criterion of the Akaike Information Criterion (AIC) and the Root-Mean-Square Error (RMSE) were adopted to select the most suitable copula from the three Archimedean copulas [52]. The Archimedean copula with the lower AIC and RMSE values indicated better fit to the joint distributions of seasonal NDVI and P/T and superior performance.

2.4.3. Identify Change Points

The Copula-based Likelihood-ratio method (CLR) was utilized to identify the change points of the relationship between seasonal NDVI and P/T. For a time series of $(x_1, y_1), \dots, (x_n, y_n)$, if only one change point of the relationship between seasonal NDVI and P/T series exists, the null hypothesis (H_0) and alternative hypothesis (H_1) are expressed as follows:

$$H_0: \lambda_1 = \lambda_2 = \dots = \lambda_n; H_1: \lambda_1 = \dots = \lambda_{k^*} \neq \lambda_{k^*+1} = \dots = \lambda_n. \quad (2)$$

If the null hypothesis is rejected, k^* is the corresponding time of the change point. When $k^* = k$ is known, the logarithmic likelihood ratio statistics of copula based on the maximum likelihood estimation method can be formed as:

$$-2 \log \Lambda_k = 2 \left[\sum_{i=1}^k \log C_{12}(\lambda_k; F(x_i), G(y_i)) + \sum_{i=k+1}^n \log C_{12}(\lambda_{k^*}; F(x_i), G(y_i)) - \sum_{i=1}^n \log C_{12}(\lambda_n; F(x_i), G(y_i)) \right] \quad (3)$$

where $F(x)$ and $G(y)$ are the probability distribution function of seasonal NDVI and P/T series, respectively. C_{12} represents the joint distribution function of seasonal NDVI and P/T series. λ_k , λ_{k^*} , and λ_n denote the parameter λ of the joint distribution of the seasonal NDVI and P/T series which is estimated by the maximum likelihood method. Considering the fitting effects of the relevant marginal and joint distributions, the range of k is confined as 6 and $n-5$.

If k^* is unknown, then

$$Z_n = \max_{6 \leq k \leq n-5} (-2 \log \Lambda_k). \quad (4)$$

When the statistic Z_n , which follows the chi square distribution, is large enough to reject the null hypothesis, a change point of the relationship between seasonal NDVI and P/T on the basis of Archimedean Copula was determined. Introduced in da Costa Dias [53], the threshold of the statistic Z_n is approximately 8.8. The time of the change point can be assessed as follows:

$$k^* = \arg \max_{6 \leq k \leq n-5} (-2 \log \Lambda_k). \quad (5)$$

2.5. Correlation Analysis

Pearson correlation coefficients were computed to access the relationship between climate change and the relationships between seasonal NDVI and P/T (denoted by Z_n series). The correlation coefficients can be written as:

$$R_{xy} = \frac{\sum_{i=1}^n [(x_i - \bar{x}) \times (y_i - \bar{y})]}{\sqrt{\sum_{i=1}^n [(x_i - \bar{x})^2 \times (y_i - \bar{y})^2]}}, \quad (6)$$

where R_{xy} is the correlation coefficient, x and y represent the seasonal values of two variables, and \bar{x} and \bar{y} are the average of the two variables. n is the length of the time period.

The overall methodology adopted in the current study is presented in Figure 2. First, the temporal trend is assessed by the MMK method. Then, the change point was identified by the copula-based

framework and the double-mass curve method. Additionally, the Pearson correlation coefficient analysis was used for the attribution analysis.

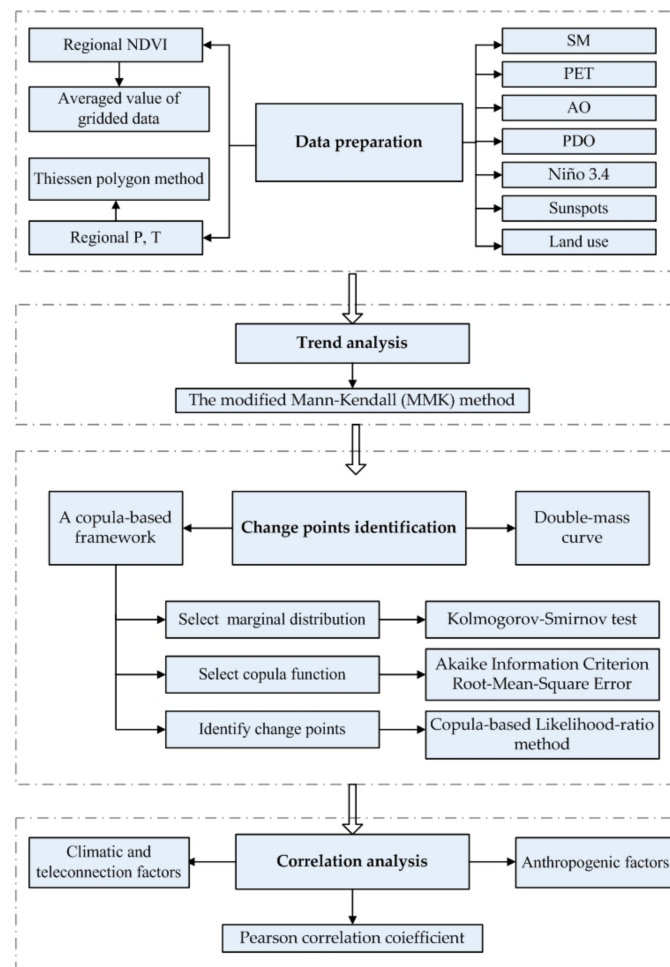


Figure 2. Flowchart of the framework for the change point identification.

3. Results

3.1. Temporal Change of Seasonal NDVI, Precipitation, and Temperature

The seasonal NDVI series covering 1982–2010 in the JRB is plotted in Figure 3. It can be roughly observed that NDVI in three seasons exhibited a noticeably increasing trend with fluctuation, and the maximum increase rate was found in autumn (0.0023/year). The MMK statistics of NDVI in spring, summer, and autumn are 0.8, 1.4, and 4.1, respectively (Table 1), which means the autumn NDVI had a statistically significant upward trend at the 99% confident level, whereas spring NDVI and summer NDVI had a non-significant increasing trend. It has been documented that vegetation growth exhibited time-lag responses to climate variations [54,55]. Thereby, the correlation coefficients between the NDVI and P/T were computed by considering the time-lag effects. The results revealed that spring NDVI had the greatest correlation with the previous 1–2 months accumulative precipitation and average temperature, and the coefficients were 0.49 and 0.38, respectively. Summer NDVI exhibited a one month lag with precipitation and no lag with temperature. In autumn, the time-lag of NDVI to precipitation and temperature was previous 0–1 month and 0–3 months, respectively (0 represented the current month). Consequently, the long-term precipitation and temperature series mentioned in this study were the corresponding series with time-lag effects taken into account. As shown in Table 1, precipitation in the three seasons showed a non-significant trend, while temperature had a

remarkable upward trend at the 95% confident level in autumn and at the 99% confident level in spring and summer. Generally, seasonal vegetation coverage and temperature in the JRB have obviously increasing trends, while precipitation has a non-significant trend.

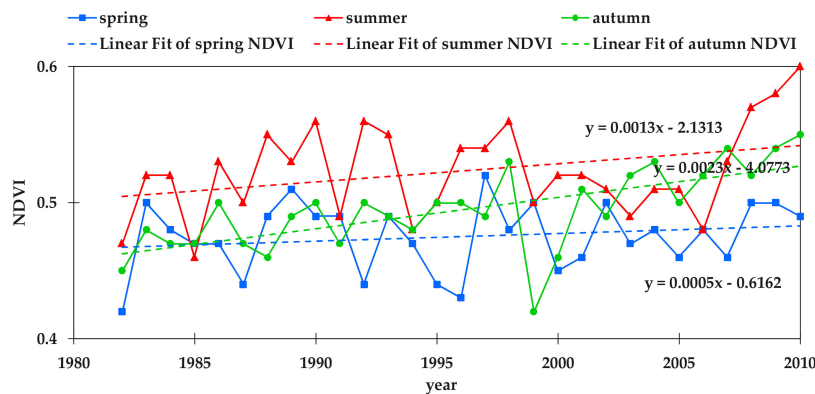


Figure 3. The seasonal Normalized Difference Vegetation Index (NDVI) and precipitation/temperature (P/T) series covering 1982–2010 in the Jing River Basin (JRB).

Table 1. The results of the modified Mann–Kendall (MMK) trend test.

Season	NDVI	P	T
Spring	0.8	−1.0	2.6 **
Summer	1.4	0.3	3.6 **
Autumn	4.1 **	0.8	2.2 *

Note: “*” and “**” represent significant at 95% and 99% confidence level, respectively.

3.2. The Selection of the Appropriate Marginal Distribution

In this study, Gamma distribution, GEV distribution, and lognormal distribution were chosen to fit the seasonal NDVI and P/T series, and then the most appropriate marginal distributions were obtained. The goodness-of-fit values of the three probability distributions were calculated by the K-S method and are shown in Table 2. Apparently, the *H* values of all the selected distributions are 0, indicating that all three distributions passed the K-S test in fitting seasonal NDVI and P/T series. In general, the results demonstrated that the *p*-values of the GEV distribution were the largest among the three distributions in fitting the seasonal NDVI and P/T, except in fitting spring temperature and autumn NDVI. Therefore, the lognormal distribution which was shown to have the maximum *p*-value in fitting spring temperature and autumn NDVI was selected as the most appropriate marginal distribution for spring temperature and autumn NDVI, while the GEV distribution was chosen as the most appropriate marginal distribution for the other time series.

Table 2. The goodness-of-fit values of the three probability distributions in fitting the distribution of individual seasonal NDVI and P/T series.

Seasons	Series	Gamma Distribution		GEV Distribution		Lognormal Distribution	
		<i>H</i>	<i>P</i>	<i>H</i>	<i>P</i>	<i>H</i>	<i>P</i>
Spring	NDVI	0	0.56	0	0.84	0	0.58
	P	0	0.92	0	0.96	0	0.70
	T	0	0.92	0	0.79	0	0.93
Summer	NDVI	0	0.97	0	0.99	0	0.98
	P	0	0.50	0	0.68	0	0.66
	T	0	0.79	0	0.95	0	0.81

Table 2. Cont.

Seasons	Series	Gamma Distribution		GEV Distribution		Lognormal Distribution	
		<i>H</i>	<i>P</i>	<i>H</i>	<i>P</i>	<i>H</i>	<i>P</i>
Autumn	NDVI	0	0.82	0	0.52	0	0.83
	P	0	0.93	0	0.98	0	0.75
	T	0	0.62	0	0.94	0	0.64

Note: *H* represents the hypothesis test result, returned as a logical value, if $H = 0$, indicating a failure to reject the null hypothesis at 95% confident level, if $H = 1$, indicating the rejecting of the null hypothesis at 95% confident level; *P* denotes the *p*-value of the test, returned as a scalar value in the range (0, 1), small values of *P* cast doubt on the validity of the null hypothesis. The bold letters represent the most appropriate marginal distributions.

3.3. The Selection of the Appropriate Copula Function

When the most appropriate marginal distribution was determined, the *RMSE* and *AIC* method were utilized to select the most appropriate copula from the Archimedean copulas (including Clayton, Frank, and Gumbel copulas) which were chosen to fit the joint distributions of seasonal NDVI and P/T in the current study. The values of the *RMSE* and *AIC* are presented in Table 3. According to the minimum criterion of *AIC* and *RMSE*, the Clayton copula is the most appropriate copula in fitting the joint distribution of spring NDVI and temperature series, and the joint distribution of autumn NDVI and precipitation series. Whereas, the *RMSE* and *AIC* values of the Frank copula in fitting other NDVI and climatic series are the lowest, indicating that Frank copula is the most appropriate copula for other joint distribution of NDVI and temperature/precipitation in the JRB (Table 3).

Table 3. The Root-Mean-Square Error (*RMSE*) and Akaike Information Criterion (*AIC*) value of Clayton, Frank, and Gumbel copulas in fitting the joint distribution of seasonal NDVI and P/T.

Seasons	Series	Clayton		Frank		Gumbel	
		<i>RMSE</i>	<i>AIC</i>	<i>RMSE</i>	<i>AIC</i>	<i>RMSE</i>	<i>AIC</i>
Spring	NDVI-P	0.029	−203.27	0.024	−215.21	0.032	−198.52
	NDVI-T	0.021	−220.40	0.022	−219.07	0.025	−212.54
Summer	NDVI-P	0.030	−202.32	0.021	−222.29	0.023	−217.82
	NDVI-T	0.032	−197.77	0.024	−214.24	0.032	−197.77
Autumn	NDVI-P	0.017	−233.95	0.022	−218.85	0.032	−197.71
	NDVI-T	0.033	−196.74	0.030	−201.06	0.040	−185.00

Note: The bold letters represent the most appropriate copula which was chosen to fit the joint distributions of seasonal NDVI and P/T in the current study.

3.4. The Identification of Change Points in the Relationship between NDVI and P/T

The copula-based method was adopted to detect the change points of the relationship between seasonal NDVI and P/T in the JRB, and the statistics of the copula-based method are shown in Figure 4. It was found that the statistic (*Z* values) of the NDVI-P in the three seasons in the 1982–2010 range from 0.1 to 2.1, 0 to 2.8 and 0.5 to 5.2, respectively, and the largest *Z* values in spring, summer, and autumn were 2.1 (2002), 2.8 (1998), and 5.2 (1988), respectively. Evidently, the largest statistics were all less than the threshold of rejecting null hypothesis (approximately 8.8), thus, no change point was detected between seasonal NDVI and P in the JRB during 1982–2010. For the relationship between NDVI and T in the JRB, the largest *Z* values in spring, summer and autumn were 5.2 (1992), 1.9 (1994), and 3.3 (1990), respectively. Similarly, no statistic was larger than the threshold of rejecting the null hypothesis. Therefore, the relationships between seasonal NDVI and P/T are still stationary under the backdrop of the changing environment. Although there were no change points between autumn NDVI and P and spring NDVI and T, their relationships might have experienced slight variations due to the relatively large *Z*_{max} value which was 5.2 for both autumn NDVI-P and spring NDVI-T. Generally,

the relationships between seasonal NDVI and P/T in the JRB fluctuated with no remarkable changing point during 1982–2010.

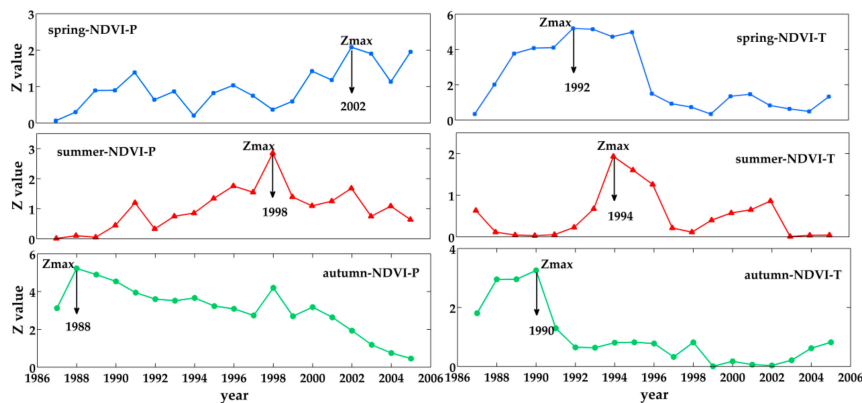


Figure 4. The statistics of copula-based method in detecting the change points of the relationship between seasonal NDVI and P/T during 1982–2010 in the JRB.

4. Discussion

4.1. Methodology

Climate change (P and T) has proven to be the primary driving force inducing the vegetation variation. For a long-term period, if there is no disturbance, the relationship between climate change and vegetation variation will remain in a steady-state. However, it is evidenced that temperature and precipitation are fluctuating unsteadily under a changing environment [7–11]. Therefore, the steady-state of the relationship between climate change and vegetation tends to be unstable. Most previous studies have focused on the statistical methods to identify the relationships without considering their non-linearity and non-stationary [22–24]. In the current study, a copula-based method was proposed to determine whether the relationship between climate change and vegetation has changed. Moreover, previous studies have adopted this copula-based method to the identification of the change points of the relationship between annual runoff and sediment series, annual rainfall and runoff [56].

In order to further verify the reliability of the results obtained by the copula-based method, the double mass curve, which is known as a relatively simple and practical method to investigate the consistency and tendency of the hydrometeorological series [56], was employed in the present study to further check the variations of the relationships between seasonal NDVI and P/T (Figure 5). It was obvious that the double-mass curve for the spring NDVI and P experienced a larger slope during 2003–2010 than during 1982–2002, which indicated that the relationship between spring NDVI and P in 1982–2002 was different from that in 1988–2010. This finding further verified that the time corresponding to the maximum Z value was the year when the relationship between spring NDVI and P began to change. Similarly, it can be observed in Figure 5 that the slope of the double mass curve for spring NDVI and T in 1992–2010 was smaller than that in 1982–1991. Thus, the relationship between spring NDVI and T began to vary in 1992, which was highly consistent with the year when Z value peaked (5.2). For the relationship between autumn NDVI and P, it can be also observed that the relationship for 1988–2010 was different from that for 1982–1987 as the slopes of the double mass curve in the two periods were different, and 1988 happened to be the year when the Z value peaked (5.2). Conversely, the slopes of the double mass curves of summer NDVI and P/T, autumn NDVI and T did not exhibit any variations during 1982–2010, indicating that the relationships of them were stationary from 1982 to 2010. Meanwhile, the Z values of the relationships between summer NDVI and P/T and autumn NDVI and T were found to be relatively small compared to other relationships analyzed above. Therefore, the results obtained by the double-mass curve were consistent with that obtained by the

copula-based method. Consequently, according to the double mass curve, the reliability and accuracy of the copula-based method applied in this study was further verified.

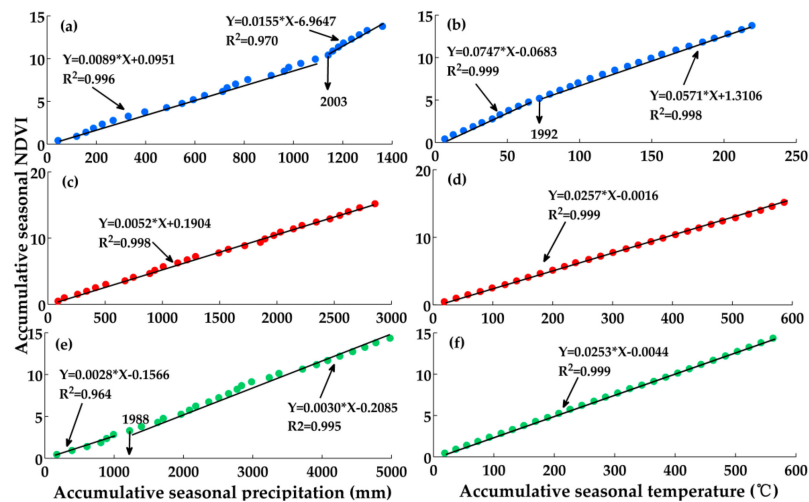


Figure 5. The double mass curves of seasonal NDVI and P/T covering 1982–2010 in the JRB. (a) and (b) represent the double-mass curve of spring NDVI-P/T; (c,d) represent the double-mass curve of summer NDVI-P/T; (e,f) represent the double-mass curve of autumn NDVI-P/T.

4.2. The Climatic Drivers for the Variations of the Relationship between NDVI and P/T

It has been proven that the large-scale atmospheric circulation anomaly and sunspots exhibited strong associations with P and T at regional and global scales [57,58]. Besides, SM and PET play important roles in vegetation dynamics [59,60]. Thereby, both the climatic and teleconnection factors might disturb the relationship between NDVI and P/T. To further identify the potential drivers at seasonal scale, two climatic variables (including SM and PET) and four teleconnection factors (including AO, PDO, Niño3.4, and sunspots) were selected and the Pearson correlation analysis was performed to investigate the detailed linkages between climatic/teleconnection factors and the relationship between NDVI and P/T (represented by the Z values which were obtained in Section 3.4). Specifically, the interaction between teleconnection factors and Z value series varied over time scales. Therefore, teleconnection factors at different time scales had different impacts on the Z value series due to their specifically strongly periodic fluctuations. Based on the above, the continuous wavelet transform analysis was utilized to detect the periodicity of long-term AO, PDO, Niño3.4, and sunspots series [61]. Results indicated that AO, PDO, Niño3.4, and sunspots series had 14a, 7a, 18a, and 11a periodicity, respectively. In order to eliminate the possible influence of the periodicity of the teleconnection factors on the results, we thereby took 14a, 7a, 18a, and 11a as the corresponding length of the moving windows to generate new stationary series of AO, PDO, Niño3.4, and sunspots which synchronized with the Z value series covering 1987–2005. Accordingly, the Pearson correlation coefficients between the climatic/teleconnection factors and Z value series were calculated to trace the sensitivity of the Z value to different climate variations, and the results are presented in Table 4.

Obviously, the spring Z_{NDVI-P} series had statistically significant correlations ($p < 0.01$) with AO, PDO, Niño3.4, as well as sunspots, while the spring Z_{NDVI-T} series was significantly correlated with AO and PDO indices ($p < 0.01$). Similarly, there were certain correlations between the autumn Z_{NDVI-P} series and all these teleconnection factors ($p < 0.01$), and the correlations were characterized by negative values for PDO and positive values for AO, Niño3.4, and sunspots. Moreover, for the autumn Z_{NDVI-T} series, AO, PDO, and Niño3.4 showed remarkable correlations with it ($p < 0.01$). These findings indicated that relationships between NDVI and P/T were closely associated with teleconnection factors in the JRB. Nevertheless, summer Z_{NDVI-P} series was not only significantly related to PDO ($p < 0.01$), but also significantly correlated with PET ($p < 0.05$). Additionally, the relationships between summer

Z_{NDVI-P} series and PDO/PET were positive. This implied that climatic factors such as PET could promote the variation of the relationship between NDVI and P in summer. It was notable that all the six selected factors had no significant correlation with the summer Z_{NDVI-T} series. This finding directly demonstrated that variation of the relationship between summer NDVI and T had no significant correlations with climatic and teleconnection factors. That is, other factors might affect the variation of the relationship between NDVI and P/T during 1982–2010 due to their complexity and uncertainty which deserves further study in the future.

Table 4. The correlations between climatic/teleconnection factors and Z value series in the JRB.

Climatic and Teleconnection Factors	Spring		Summer		Autumn	
	Z_{NDVI-P}	Z_{NDVI-T}	Z_{NDVI-P}	Z_{NDVI-T}	Z_{NDVI-P}	Z_{NDVI-T}
SM	−0.28	−0.14	−0.32	0.31	−0.22	0.17
PET	0.20	−0.24	0.46 *	0.24	−0.09	−0.10
AO	−0.65 **	0.72 **	−0.43	0.38	0.71 **	0.58 **
PDO	0.61 **	−0.71 **	0.51 *	−0.14	−0.78 **	−0.65 **
Niño3.4	−0.71 **	0.15	0.04	0.19	0.78 **	0.48 *
Sunspots	−0.72 **	0.41	−0.31	0.39	0.74 **	0.43
EIA	0.26	0.09	0.61 **	0.39	0.41	0.84 **

Note: “*” and “**” represent significant at 95% and 99% confidence level, respectively. The bold numbers represent the significant correlations between climatic/teleconnection factors and Z value series.

According to this research, relationships between seasonal NDVI and P/T were sensitive to the teleconnection factors over the past three decades, especially in spring and autumn. This result is consistent with those of related studies, which have shown clearly the essential roles that teleconnection factors played on vegetation variations in spring/autumn vegetation and climate variations. Anyamba and Eastman [62] found that strong spatial and temporal teleconnection patterns exist between ENSO related climate anomalies and patterns of variation in NDVI. Cho et al. [58] revealed that 17% of the spring vegetation variance was explained by the previous winter’s AO variations over the total northern high latitudes, emphasizing the importantly predictive role that winter AO on the vegetation greenness or dynamics in subsequent spring. Moreover, global climate anomalies (such as displacements in the rainfall patterns) were proven to be teleconnected with the anomalous warming of oceanic waters and changes in the Walker circulation [62]. Therefore, the large-scale atmospheric circulation anomaly which coupled the ocean-atmosphere system has a significant influence on climate change. Gong and Shi [63] have addressed that large-scale climate systems such as ENSO and AO can significantly influence the inter-annual variations of regional temperature, especially the temperature in spring. Previous studies have demonstrated that temperature change could result in noticeably biological consequences, including lengthened growing season, promoted vegetation activity, and greater biomass productivity [64,65]. Therefore, by changing the regional temperature, the large-scale climate fluctuations affect the vegetation coverage. Consequently, the direct impacts of teleconnection factors on climate change and indirect impacts of teleconnection factors on vegetation coverage jointly affect the relationship between NDVI and P/T.

Observations during 1982–2010 have shown a rising trend in seasonal temperature in the JRB, especially in summer. The increase in summer temperature could accelerate evapotranspiration and decrease soil moisture, resulting in drought and inhibition of vegetation growth. Additionally, the JRB is widely known as a water-limited region and the vegetation in water-limited region is sensitive to precipitation [7,66]. However, the precipitation in summer covering 1982–2010 in the JRB has a non-significant trend. Therefore, in the context of poor precipitation and high temperature in summer, the relationship between NDVI and P/T in summer is more sensitive to high intensity evapotranspiration and soil moisture loss than in other seasons.

Briefly, considering the important role climatic and teleconnection factors play on vegetation and P/T variations, the deep exploration of their relationships helps better reveal and understand their evolutionary characteristics, thus contribute to more robust predictions of future climate and ecosystem.

4.3. The Anthropogenic Drivers for the Variations of the Relationship between NDVI and P/T

Although climatic factors have remarkable impacts on the variations of the relationship between NDVI and P/T, the important role of human activity on vegetation dynamics cannot be overlooked which tend to influence the relationship between NDVI and P/T.

Based on the land use data and map illustrated in Table 5 and Figure 6, it was easily found that farmland, forestland, and grassland were three main land types in the JRB which together accounted for more than 95% of the total area during 1980–2010. However, their respective areas have experienced fluctuated variations between 1980 and 2010. It has been reported that the population in the JRB increased rapidly during 1990–1995 [67], resulting in the inevitably increased demand for farmland and the accelerated urban expansion [68]. Therefore, the grassland and water area were converted to farmland to meet the food demand in the context of population explosion. It can be obviously seen from Table 5 that grassland and water area decreased during 1990–1995, while farmland and construction land increased significantly. On the other hand, the rapid growth of population and urban expansion could also lead to overgrazing and excessive wood cutting, and thus reducing the forestland area during 1990–1995. Consequently, human activities mainly played a destructive role in vegetation, resulting in vegetation degradation in the JRB during 1990–1995.

Table 5. Characteristics of inter-annual variations of land-cover in the JRB.

Year	Farmland		Forestland		Grassland		Water Bodies		Construction Land		Unused Land	
	Area km ²	Ratio %	Area km ²	Ratio %	Area km ²	Ratio %	Area km ²	Ratio %	Area km ²	Ratio %	Area km ²	Ratio %
1980	19,901	44.41	4179	9.33	19,829	44.25	215	0.48	690	1.54	1	0
1990	19,960	44.54	4239	9.46	19,738	44.04	205	0.46	670	1.49	3	0.01
1995	20,172	45.01	4023	8.98	19,645	43.84	192	0.43	721	1.61	62	0.14
2000	19,865	44.33	4026	8.98	19,946	44.51	213	0.47	765	1.71	0	0
2005	19,499	43.51	4439	9.9	19,815	44.22	212	0.47	847	1.89	3	0.01
2010	19,426	43.35	4470	9.97	19,847	44.29	209	0.47	860	1.92	3	0.01

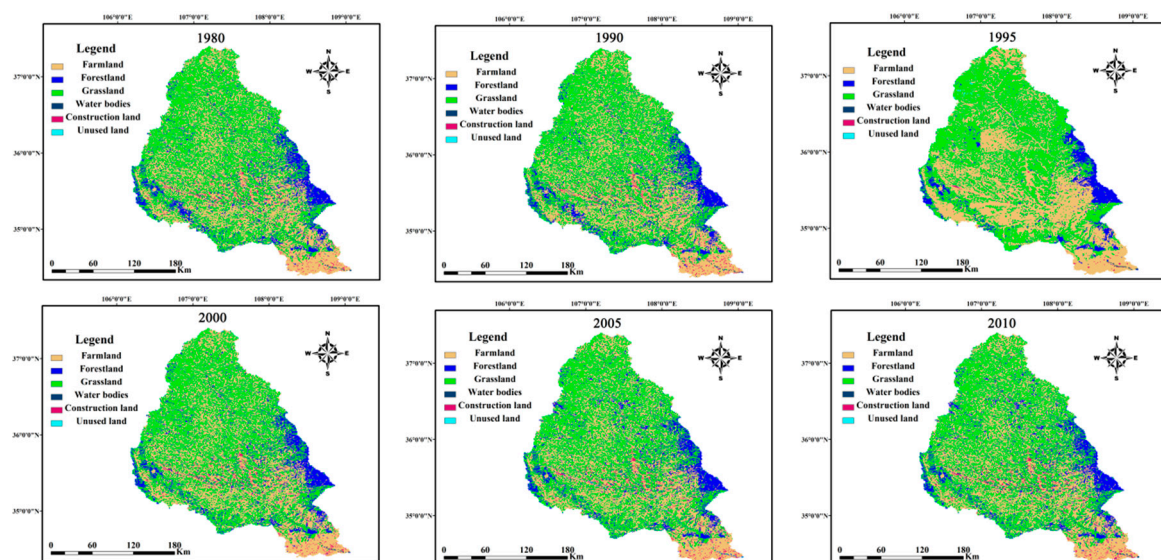


Figure 6. Land use map in different periods of the Jing River Basin.

It is well known that the JRB has experienced intensive soil erosion, with an average of nearly 2.6×10^8 t of sediment transported into the JRB per year, accounting for 14% of the annual sediment load in the YRB [37]. Hence, a series of water and soil conservation measures have been implemented on the Loess Plateau which contains the JRB to reduce the soil erosion rate, especially the “Grain for Green” program (GGP) launched by the Chinese government in 1999 [69]. The improvement of vegetation coverage and the alteration of land cover patterns jointly affected the land surface hydrological processes through intercepting precipitation and promoting the infiltration rate [70]. The current study confirmed that the farmland area exhibited a decreasing trend during 1995–2005, while the forestland and grassland area increased during 1995–2005 (Table 5). This is in accordance with the previous research on the Loess Plateau [71,72]. Xiao [71] found a significant GGP-induced increase in the leaf area index and tree coverage on the Loess Plateau. Tang et al. [72] noted a significant decrease in the farmland areas and a significant increase in the forest areas on the Loess Plateau. Therefore, human activities such as the GGP could have obviously promoted the vegetation coverage during 1995–2005.

In conclusion, both the negative and positive human disturbances affect vegetation growth, and their impacts on vegetation were more direct and efficient than climatic factors. Besides, human activities indirectly regulate the climate of a basin by affecting vegetation growth. Therefore, the variations of relationship between NDVI and P/T during 1982–2010 were closely associated with human activities in the JRB. Furthermore, based on the effective irrigated area data (EIA), the correlation coefficients between seasonal Z value series and EIA were calculated and the results are presented in Table 4. Obviously, the EIA was significantly positively correlated with the summer Z_{NDVI-P} series and autumn Z_{NDVI-T} series ($p < 0.01$), indicating that human activities such as EIA could promote the relationship changes between NDVI and P/T in summer and autumn. Consequently, considering anthropogenic disturbances will be helpful for deeper investigating the possible non-stationarity of the relationship between vegetation growth and climate change under a changing environment, thus revealing the detailed attributions.

5. Conclusions

Climate disturbance played a crucial role in vegetation dynamics under the background of a changing environment. Therefore, understanding the variation of their relationships and identifying the change points of the relationships was an important basis to evaluate the potential influence of climate change on ecosystems which will support regional land planning and management.

In this study, temporal variations of NDVI, P, and T were investigated in the JRB which is widely known as a typical arid and semi-arid region in China. According to the MMK test, the seasonal T and autumn NDVI exhibited a significant increasing trend, whilst P showed an insignificant trend during 1982–2010 in the JRB. Besides, a copulas-based method was introduced in present study to detect the possible change points between NDVI and P/T. Simultaneously, the double-mass curves method was adopted to verify the reliability of the results acquired by the copula-based method. The two methods consistently showed that the relationships between spring NDVI and P/T and autumn NDVI and P basin have slightly changed, while the relationships of summer NDVI-P/T and autumn NDVI-P have not strikingly changed in the JRB. Generally, no significant change point was identified from the relationship between seasonal NDVI and P/T. We further revealed the dominant drivers of the fluctuations of the relationships between NDVI and P/T at seasonal scales by considering the large-scale atmospheric circulation systems. On average, teleconnection factors have significant impacts on the relationship between seasonal NDVI and P/T. Additionally, the human-induced vegetation degradation and vegetation greenness showed a remarkable influence on the variations of the relationship between NDVI and P/T.

In conclusion, a new framework was proposed in the present study to explore the non-stationarity of the relationship between seasonal NDVI and P/T, which could help effectively and reliably investigate the sensitivity of vegetation dynamics to climate change, thus conducting ecological restoration on vegetation cover at regional scales.

Author Contributions: Conceptualization, J.Z., S.H., Q.H., H.W., G.L., J.P. and H.D.; data curation, G.L. and S.H.; methodology and formal analysis, J.Z. and H.D.; writing—original draft preparation, J.Z.; writing—review and editing, S.H., Q.H., and G.L.

Funding: This research was supported by the National Key Research and Development Program of China (grant number 2017YFC0405900), the National Natural Science Foundation of China (grant number 51709221), the Planning Project of Science and Technology of Water Resources of Shaanxi (grant numbers 2015slkj-27 and 2017slkj-19), the China Scholarship Council (grant number 201508610099), the Belt and Road Special Foundation of the State Key Laboratory of Hydrology-Water Resources and Hydraulic Engineering (grant number 2018490711), the Open Research Fund of State Key Laboratory of Simulation and Regulation of Water Cycle in River Basin (China Institute of Water Resources and Hydropower Research, grant number IWHR-SKL-KF201803 and the Doctorate Innovation Funding of Xi'an University of Technology (grant number 310-252071712).

Acknowledgments: In this study, the NDVI data, meteorological data, and teleconnection data were download from different data centers. The authors express their gratitude for the data sharing of the above datasets. Moreover, sincere gratitude is extended to the editor and the anonymous reviewers who provided professional comments for this paper.

Conflicts of Interest: The authors declare no conflict of interest.

References

- Peng, S.-S.; Piao, S.; Zeng, Z.; Ciais, P.; Zhou, L.; Li, L.Z.X.; Myneni, R.B.; Yin, Y.; Zeng, H. Afforestation in China cools local land surface temperature. *Proc. Natl. Acad. Sci. USA* **2014**, *111*, 2915–2919. [[CrossRef](#)] [[PubMed](#)]
- Piao, S.; Nan, H.; Huntingford, C.; Ciais, P.; Friedlingstein, P.; Sitch, S.; Peng, S.; Ahlström, A.; Canadell, J.G.; Cong, N.; et al. Evidence for a weakening relationship between interannual temperature variability and northern vegetation activity. *Nat. Commun.* **2014**, *5*, 1–7. [[CrossRef](#)] [[PubMed](#)]
- Pielke, R.A. Land use and climate change. *Science* **2005**, *310*, 1625–1626. [[CrossRef](#)] [[PubMed](#)]
- Sterling, S.M.; Ducharne, A.; Polcher, J. The impact of global land-cover change on the terrestrial water cycle. *Nat. Clim. Change* **2013**, *3*, 385–390. [[CrossRef](#)]
- Udelhoven, T.; Stellmes, M.; Barrio, G.; Hill, J. Assessment of rainfall and NDVI anomalies in Spain (1989–1999) using distributed lag models. *Int. J. Remote Sens.* **2009**, *30*, 1961–1976. [[CrossRef](#)]
- Huber, S.; Fensholt, R.; Rasmussen, K. Water availability as the driver of vegetation dynamics in the African Sahel from 1982 to 2007. *Glob. Planet Change* **2011**, *76*, 186–195. [[CrossRef](#)]
- Zhao, J.; Huang, S.; Huang, Q.; Wang, H.; Leng, G. Detecting the dominant cause of streamflow decline in the Loess Plateau of china based on the latest budyko equation. *Water* **2018**, *10*, 1277. [[CrossRef](#)]
- Liu, L.; Huang, G.; Baetz, B.; Zhang, K. Environmentally-extended input-output simulation for analyzing production-based and consumption-based industrial greenhouse gas mitigation policies. *Appl. Energy* **2018**, *232*, 69–78. [[CrossRef](#)]
- Ciais, P.; Reichstein, M.; Viovy, N.; Granier, A.; Ogèe, J.; Allard, V.; Aubinet, M.; Buchmann, N.; Bernhofer, C.; Carrara, A.; et al. Europe-wide reduction in primary productivity caused by the heat and drought in 2003. *Nature* **2005**, *437*, 529–533. [[CrossRef](#)]
- De Keersmaecker, W.; Lhermitte, S.; Tits, L.; Honnay, O.; Somers, B.; Coppin, P. A model quantifying global vegetation resistance and resilience to short-term climate anomalies and their relationship with vegetation cover cover. *Glob. Ecol. Biogeogr.* **2015**, *24*, 539–548. [[CrossRef](#)]
- Yang, Y.; Piao, S. Variations in grassland vegetation cover in relation to climatic factors on the Tibetan Plateau. *J. Plant Ecol.* **2006**, *30*, 1–8. [[CrossRef](#)]
- Wang, X.; Xie, H.; Guan, H.; Zhou, X. Different responses of MODIS-derived NDVI to root-zone soil moisture in semi-arid and humid regions. *J. Hydrol.* **2007**, *340*, 12–24. [[CrossRef](#)]
- Yu, Z.; Carlson, T.N.; Barron, E.J.; Schwartz, F.W. On evaluating the spatial-temporal variation of soil moisture in the Susquehanna river basin. *Water Resour. Res.* **2001**, *37*, 1313–1326. [[CrossRef](#)]
- Jiménez-Muñoz, J.C.; Sobrino, J.A.; Gillespie, A.; Sabol, D.; Gustafson, W.T. Improved land surface emissivities over agricultural areas using ASTER NDVI. *Remote Sens. Environ.* **2006**, *103*, 474–487. [[CrossRef](#)]
- Boegh, E.; Soegaard, H. Remote sensing based estimation of evapotranspiration rates. *Int. J. Remote Sens.* **2004**, *25*, 2535–2551. [[CrossRef](#)]
- Jiang, L.; Islam, S. Estimation of surface evaporation map over southern Great Plains using remote sensing data. *Water Resour. Res.* **2001**, *37*, 329–340. [[CrossRef](#)]

17. Zeng, B.; Yang, T.B. Natural vegetation responses to warming climates in Qaidam Basin 1982–2003. *Int. J. Remote Sens.* **2009**, *30*, 5685–5701. [[CrossRef](#)]
18. Yan, D.; Xu, T.; Girma, A.; Yuan, Z.; Weng, B.; Qin, T.; Do, P.; Yuan, Y. Regional correlation between precipitation and vegetation in the Huang-Huai-Hai river basin, China. *Water* **2017**, *9*, 557. [[CrossRef](#)]
19. Shen, B.; Fang, S.; Li, G. Vegetation coverage changes and their response to meteorological variables from 2000 to 2009 in Naqu, Tibet, China. *Can. J. Remote Sens.* **2014**, *40*, 67–74. [[CrossRef](#)]
20. Wen, Y.; Liu, X.; Pei, F.; Li, X.; Du, G. Non-uniform time-lag effects of terrestrial vegetation responses to asymmetric warming. *Agric. For. Meteorol.* **2018**, *252*, 130–143. [[CrossRef](#)]
21. Ji, L.; Peters, A.J. Assessing vegetation response to drought in the northern Great Plains using vegetation and drought indices. *Remote Sens. Environ.* **2003**, *87*, 85–98. [[CrossRef](#)]
22. Favretto, N.; Stringer, L.C.; Dougill, A.J.; Dallimer, M.; Perkins, J.S.; Reed, M.S.; Athhopheng, J.R.; Mulale, K. Multi-criteria decision analysis to identify dryland ecosystem service trade-offs under different rangeland land uses. *Ecosyst. Serv.* **2016**, *17*, 142–151. [[CrossRef](#)]
23. Jopke, C.; Kreyling, J.; Maes, J.; Koellner, T. Interactions among ecosystem services across Europe: Bagplots and cumulative correlation coefficients reveal synergies, trade-offs, and regional patterns. *Ecol. Indic.* **2015**, *49*, 46–52. [[CrossRef](#)]
24. Jin, X.; Hao, Z.; Zhang, J. Study on the relation of frequency between flood and sediment in the middle Yellow River. *J. Sediment Res.* **2006**, *3*, 41–43. [[CrossRef](#)]
25. Hao, R.; Yu, D.; Wu, J. Relationship between paired ecosystem services in the grassland and agro-pastoral transitional zone of China using the constraint line method. *Agric. Ecosyst. Environ.* **2017**, *240*, 171–181. [[CrossRef](#)]
26. Lee, H.; McIntyre, N.; Wheeler, H.; Young, A. Selection of conceptual models for regionalisation of the rainfall-runoff relationship. *J. Hydrol.* **2005**, *312*, 125–147. [[CrossRef](#)]
27. Birkinshaw, S.J.; Bathurst, J.C. Model study of the relationship between sediment yield and river basin area. *Earth Surf. Process. Landf.* **2006**, *31*, 750–761. [[CrossRef](#)]
28. Gu, D.; Ye, W.; Miao, B. Analysis of regional financial contagion based on vine copula method. *J. Univ. Sci. Technol. Chin.* **2013**, *43*, 737–744. [[CrossRef](#)]
29. Huang, S.; Huang, Q.; Zhang, H.; Chen, Y.; Leng, G. Spatio-temporal changes in precipitation, temperature and their possibly changing relationship: A case study in the Wei River Basin, China. *Int. J. Climatol.* **2016**, *36*, 1160–1169. [[CrossRef](#)]
30. Ye, W.; Miao, B.; Ma, Y. Analysis of sub-prime loan crisis contagion based on change point testing method of hazard function. *Syst. Eng. Theory Pract.* **2010**, *30*, 431–436. [[CrossRef](#)]
31. Huang, S.; Huang, Q.; Chang, J.; Leng, G. Linkages between hydrological drought, climate indices and human activities: a case study in the Columbia River basin. *Int. J. Climatol.* **2016**, *36*, 280–290. [[CrossRef](#)]
32. Han, Z.; Huang, S.; Huang, Q.; Leng, G.; Wang, H.; He, L.; Fang, W.; Li, P. Assessing GRACE-based terrestrial water storage anomalies dynamics at multi-timescales and their correlations with teleconnection factors in Yunnan Province, China. *J. Hydrol.* **2019**. [[CrossRef](#)]
33. Huang, S.; Li, P.; Huang, Q.; Leng, G.; Hou, B.; Ma, L. The propagation from meteorological to hydrological drought and its potential influence factors. *J. Hydrol.* **2017**, *547*, 184–195. [[CrossRef](#)]
34. Li, J.; Fan, K.; Zhou, L. Satellite observations of El Niño impacts on Eurasian spring vegetation greenness during the period 1982–2015. *Remote Sens.* **2017**, *9*, 628. [[CrossRef](#)]
35. Cavazos, T. Using self-organizing maps to investigate extreme climate events: An application to wintertime precipitation in the Balkans. *J. Clim.* **2000**, *13*, 1718–1732. [[CrossRef](#)]
36. Wu, B.; Wang, J. Possible impact of winter Arctic Oscillation on Siberian High, the East Asian winter monsoon and sea-ice extent. *Adv. Atmos. Sci.* **2002**, *19*, 297–320. [[CrossRef](#)]
37. Zhao, J.; Huang, Q.; Chang, J.; Liu, D.; Huang, S.; Shi, X. Analysis of temporal and spatial trends of hydro-climatic variables in the Wei river basin. *Environ. Res.* **2015**, *139*, 55–64. [[CrossRef](#)] [[PubMed](#)]
38. Liu, S.; Huang, S.; Xie, Y.; Wang, H.; Huang, Q.; Leng, G.; Li, P.; Wang, L. Spatial-temporal changes in vegetation coverage in a typical semi-humid and semi-arid region in China: Changing patterns, causes and implications. *Ecol. Indic.* **2019**, *98*, 462–475. [[CrossRef](#)]
39. Li, X.; Wei, X.; Wei, N. Correlating check dam sedimentation and rainstorm characteristics on the Loess Plateau, China. *Geomorphology* **2016**, *265*, 84–97. [[CrossRef](#)]

40. Xin, Z.; Yu, X.; Li, Q.; Lu, X.X. Spatiotemporal variation in rainfall erosivity on the Chinese Loess Plateau during the period 1956–2008. *Reg. Environ. Change* **2011**, *11*, 149–159. [[CrossRef](#)]
41. Caocao, C.; Gaodi, X.; Lin, Z.; Yunfa, L. Analysis on Jinghe watershed vegetation dynamics and evaluation on its relation with precipitation. *Acta Ecol. Sinica* **2008**, *28*, 925–938. [[CrossRef](#)]
42. Faisal, N.; Gaffar, A. Development of pakistan's new area weighted rainfall using thiesen polygon method. *Pak. J. Meteorol.* **2012**, *9*, 107–116.
43. Mitchell, J.M.; Dzerdzevskii, B.; Flohn, H.; Hofmeyr, W.L.; Lamd, H.H.; Rao, K.N.; Wallen, C.C. *Climate Change*; Technical Note No. 79; World Meteorological Organization: Geneva, Switzerland, 1966; p. 79.
44. Hamed, K.H.; Ramachandra Rao, A. A modified Mann-Kendall trend test for autocorrelated data. *J. Hydrol.* **1998**, *204*, 182–196. [[CrossRef](#)]
45. Guo, Y.; Huang, S.; Huang, Q.; Wang, H.; Fang, W.; Yang, Y.; Wang, L. Assessing socioeconomic drought based on an improved Multivariate Standardized Reliability and Resilience Index. *J. Hydrol.* **2019**, *568*, 904–918. [[CrossRef](#)]
46. Huang, S.; Chang, J.; Huang, Q.; Chen, Y. Spatio-temporal changes and frequency analysis of drought in the Wei river basin, china. *Water Resour. Manag.* **2014**, *28*, 3095–3110. [[CrossRef](#)]
47. Mathier, L.; Perreault, L.; Bobee, B. The use of geometric and gamma-related distributions for frequency analysis of water deficit. *Stoch. Hydrol. Hydraul.* **1992**, *6*, 239–254. [[CrossRef](#)]
48. Fang, W.; Huang, S.; Huang, G.; Huang, Q.; Wang, H.; Wang, L.; Zhang, Y.; Li, P.; Ma, L. Copulas-based risk analysis for inter-seasonal combinations of wet and dry conditions under a changing climate. *Int. J. Climatol.* **2018**, *39*, 2005–2021. [[CrossRef](#)]
49. Wilks, D.S. Interannual variability and extreme-value characteristics of several stochastic daily precipitation models. *Agric. For. Meteorol.* **1999**, *93*, 153–169. [[CrossRef](#)]
50. Ravens, B. An introduction to copulas. *Technometrics* **2000**, *42*, 317. [[CrossRef](#)]
51. Genest, C.; Rivest, L.P. Statistical inference procedures for bivariate Archimedean copulas. *J. Am. Stat. Assoc.* **1993**, *88*, 1034–1043. [[CrossRef](#)]
52. Akaike, H. A new look at the statistical model identification. *IEEE Trans. Autom. Control* **1974**, *19*, 716–723. [[CrossRef](#)]
53. Costa Dias, A.D. Copula Inference for Finance and Insurance. Ph.D. Thesis, SWISS FEDERAL INSTITUTE OF TECHNOLOGY ZURICH, Zurich, Switzerland, 2004. [[CrossRef](#)]
54. Gu, Z.; Duan, X.; Shi, Y.; Li, Y.; Pan, X. Spatiotemporal variation in vegetation coverage and its response to climatic factors in the Red river basin, China. *Ecol. Indic.* **2018**, *93*, 54–64. [[CrossRef](#)]
55. Ning, T.; Liu, W.; Lin, W.; Song, X. NDVI variation and its responses to climate change on the Northern Loess Plateau of China from 1998 to 2012. *Adv. Meteorol.* **2015**, *2015*, 1–10. [[CrossRef](#)]
56. Guo, A.; Chang, J.; Wang, Y.; Li, Y. Variation characteristics of rainfall-runoff relationship and driving factors analysis in Jinghe river basin in nearly 50 years. *Trans. Chin. Soc. Agric. Eng.* **2015**, *31*, 165–171. [[CrossRef](#)]
57. Li, J.; Fan, K.; Xu, Z. Links between the late wintertime North Atlantic Oscillation and springtime vegetation growth over Eurasia. *Clim. Dyn.* **2016**, *46*, 987–1000. [[CrossRef](#)]
58. Cho, M.H.; Lim, G.H.; Song, H.J. The effect of the wintertime Arctic Oscillation on springtime vegetation over the northern high latitude region. *Asia Pac. J. Atmos. Sci.* **2014**, *50*, 567–573. [[CrossRef](#)]
59. Joiner, J.; Yoshida, Y.; Anderson, M.; Holmes, T.; Hain, C.; Reichle, R.; Koster, R.; Middleton, E.; Zeng, F. Global relationships among traditional reflectance vegetation indices (NDVI and NDII), evapotranspiration (ET), and soil moisture variability on weekly timescales. *Remote Sens. Environ.* **2018**, *219*, 339–352. [[CrossRef](#)]
60. Kumar, T.V.L.; Rao, K.K.; Barbosa, H. Studies on spatial pattern of NDVI over India and its relationship with rainfall, air temperature, soil moisture adequacy and ENSO. *Geofizika* **2013**, *30*, 1–18. [[CrossRef](#)]
61. Özger, M.; Mishra, A.K.; Singh, V.P. Scaling characteristics of precipitation data in conjunction with wavelet analysis. *J. Hydrol.* **2010**, *395*, 279–288. [[CrossRef](#)]
62. Anyamba, A.; Eastman, J.R. Interannual variability of ndvi over africa and its relation to el niño/southern oscillation. *Int. J. Remote Sens.* **1996**, *17*, 2533–2548. [[CrossRef](#)]
63. Gong, D.; Shi, P. Northern hemispheric NDVI variations associated with large-scale climate indices in spring. *Int. J. Remote Sens.* **2003**, *24*, 2559–2566. [[CrossRef](#)]
64. Suzuki, R.; Tanaka, S.; Yasunari, T. Relationships between meridional profiles of satellite-derived vegetation index (ndvi) and climate over siberia. *Int. J. Climatol.* **2000**, *20*, 955–967. [[CrossRef](#)]

65. Zhou, L.; Tucker, C.J.; Kaufmann, R.K.; Slayback, D.; Shabanov, N.V.; Myneni, R.B. Variations in northern vegetation activity inferred from satellite data of vegetation index during 1981–1999. *J. Geophys. Res.* **2001**, *106*, 20069–20083. [[CrossRef](#)]
66. Wang, X.; Zhao, X.L.; Zhang, Z.X.; Yi, L.; Zuo, L.J.; Wen, Q.K.; Liu, F.; Xu, J.Y.; Hu, S.G.; Liu, B. Assessment of soil erosion change and its relationships with land use/cover change in China from the end of the 1980s to 2010. *Catena* **2016**, *137*, 256–268. [[CrossRef](#)]
67. Yang, L.; Xie, G.; Zhen, L.; Guo, G.; Leng, Y.; Ge, Y. Spatial-temporal changes of land use in Jinghe watershed. *Resour. Sci.* **2005**, *27*, 26–32. [[CrossRef](#)]
68. Pimentel, D.; Pimentel, M. Global environmental resources versus world population growth. *Ecol. Econ.* **2006**, *59*, 195–198. [[CrossRef](#)]
69. Wang, S.; Fu, B.; Piao, S.; Lü, Y.; Ciais, P.; Feng, X.; Wang, Y. Reduced sediment transport in the yellow river due to anthropogenic changes. *Nat. Geosci.* **2015**, *9*, 38–41. [[CrossRef](#)]
70. Li, Z.; Liu, W.Z.; Zhang, X.; Zheng, F. Impacts of land use change and climate variability on hydrology in an agricultural catchment on the Loess plateau of China. *J. Hydrol.* **2009**, *377*, 35–42. [[CrossRef](#)]
71. Xiao, J.F. Satellite evidence for significant biophysical consequences of the ‘Grain for Green’ Program on the Loess Plateau in China. *J. Geophys. Res. Biogeosci.* **2014**, *119*, 2261–2275. [[CrossRef](#)]
72. Tang, Q.; Xu, Y.; Liu, Y. Spatial difference of land use change in Loess plateau region. *J. Arid Land Resour. Environ.* **2010**, *24*, 15–21. [[CrossRef](#)]



© 2019 by the authors. Licensee MDPI, Basel, Switzerland. This article is an open access article distributed under the terms and conditions of the Creative Commons Attribution (CC BY) license (<http://creativecommons.org/licenses/by/4.0/>).